HHS Public Access

Author manuscript

Adv Funct Mater. Author manuscript; available in PMC 2018 October 19.

Published in final edited form as:

Adv Funct Mater. 2017 October 19; 27(39): . doi:10.1002/adfm.201703261.

Tantalum Sulfide Nanosheets as a Theranostic Nanoplatform for Computed Tomography Imaging-Guided Combinatorial Chemo-Photothermal Therapy

Yanlan Liu, Dr.,
Center for Nanomedicine and Department of Anesthesiology, Brigham and Women's Hospital, Harvard Medical School, Boston, MA 02115, USA

Xiaoyuan Ji,
Center for Nanomedicine and Department of Anesthesiology, Brigham and Women's Hospital, Harvard Medical School, Boston, MA 02115, USA; State Key Laboratory of Biochemical Engineering, Institute of Process Engineering, Chinese Academy of Sciences, Beijing 100190, China; University of Chinese Academy of Sciences, Beijing, 100049, China

Jianhua Liu,
Department of Radiology, the Second Hospital of Jilin University Norman Bethune, Changchun, 130022, China

Winnie W. L. Tong,
Center for Nanomedicine and Department of Anesthesiology, Brigham and Women's Hospital, Harvard Medical School, Boston, MA 02115, USA

Diana Askhatova, and
Center for Nanomedicine and Department of Anesthesiology, Brigham and Women's Hospital, Harvard Medical School, Boston, MA 02115, USA

Jinjun Shi, Prof.
Center for Nanomedicine and Department of Anesthesiology, Brigham and Women's Hospital, Harvard Medical School, Boston, MA 02115, USA

Abstract

Near-infrared (NIR)-absorbing metal-based nanomaterials have shown tremendous potential for cancer therapy, given their facile and controllable synthesis, efficient photothermal conversion, capability of spatiotemporal-controlled drug delivery, and intrinsic imaging function. Tantalum (Ta) is among the most biocompatible metals and arouses negligible adverse biological responses in either oxidized or reduced forms, and thus Ta-derived nanomaterials represent promising candidates for biomedical applications. However, Ta-based nanomaterials by themselves have not been explored for NIR-mediated photothermal ablation therapy. In this work, we report an innovative Ta-based multifunctional nanoplatform composed of biocompatible tantalum sulfide (TaS_2) nanosheets (NSs) for simultaneous NIR hyperthermia, drug delivery, and computed

Correspondence to: Jinjun Shi.

Supporting Information: Supporting Information is available from the Wiley Online Library or from the author.

tomography (CT) imaging. The TaS_2 NSs exhibit multiple unique features including (i) efficient NIR light-to-heat conversion with a high photothermal conversion efficiency of 39%. (ii) high drug loading (177% by weight), (iii) controlled drug release triggered by NIR light and moderate acidic pH, (iv) high tumor accumulation via heat-enhanced tumor vascular permeability, (v) complete tumor ablation and negligible side effects, and (vi) comparable CT imaging contrast efficiency to the widely clinically used agent iobitridol. We expect that this multifunctional NS platform can serve as a promising candidate for imaging-guided cancer therapy and selection of cancer patients with high tumor accumulation.

Graphical abstract

TaS_2-based cancer nanomedicine: A novel NIR-absorbing PEG-TaS_2 nanosheet platform was developed, which possesses several unique features including NIR-triggered hyperthermia, high drug loading capacity, multiple stimuli-responsive drug release, good biocompatibility, high tumor accumulation, and efficient X-ray attenuation for CT imaging. This PEG-TaS_2-based nanomedicne provides a potential new strategy for personalized treatment of advanced malignancies.

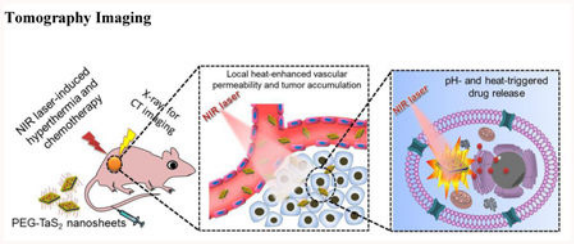

Keywords

TaS_2 nanosheet; drug delivery; hyperthermia; cancer therapy; CT imaging

1. Introduction

With high selectivity and minimal invasiveness, NIR light-induced photothermal ablation (PTA) therapy, which relies on photothermal agents to locally convert NIR irradiation into heat, has recently emerged as a powerful strategy for cancer therapy.[1] Compared to conventional NIR dyes, NIR-absorbing nanomaterials have attracted increasing attention for cancer PTA,[2] due to their improved pharmacokinetics, higher tumor accumulation by the enhanced permeability and retention (EPR) effect,[3] and better photostability. In particular, considerable efforts have been devoted to the development of metal-based (such as Au, Pt, Bi, Cu, and Fe) PTA nanomaterials,[4] given their robust synthesis, high NIR to heat conversion, and intrinsic capability of clinical CT, PET, or MRI imaging for potential real-time *in vivo* tracking and selection of cancer patients with high EPR effect.[5] However, it has been increasingly recognized that one critical limit associated with PTA nanomaterials (and other nanomedicines in general) is their inhomogeneous accumulation in the complex tumor tissues,[5-6] which could lead to large thermal gradients throughout the tumor tissue upon laser irradiation and potentially incomplete tumor ablation.[7] While increasing light irradiance may suffice the desired temperature for efficient hyperthermia, it will elicit

several issues, such as overheating-induced injury to nearby normal tissues and limiting the NIR light penetration depth if charring occurs. The loading of small molecular drugs on PTA nanomaterials has thus been proposed to compensate for this limitation, attributable to spatiotemporally controlled drug release in tumors under laser irradiance.[2c, 8]

Layered transition metal dichalcogenides (TMDs) nanomaterials, such as MoS_2, WS_2, and ReS_2, have recently demonstrated tremendous opportunities for efficient PTA and drug delivery,[4f, 9] due to their high NIR absorbance, large surface areas, and better physiological stability than conventional two-dimensional nanomaterials. Nevertheless, the potential *in vivo* toxicity regarding these transition metals remains unclear. Among the large family of TMDs, TaS_2 is expected to be of great promise for biomedical applications, as Ta is a highly biocompatible metal compared to other transition metals and triggers negligible adverse biological responses in any redox form. Ta compounds have thus been widely used in clinical implants, artificial joints, stents, and vascular clips for more than 50 years.[10] Ta also has a high atomic number and its K-edge energy locates within the uppermost energy region of the X-ray spectrum for high X-ray attenuation, which makes Ta more valuable than other transition metals for CT imaging. Moreover, unlike other Ta compounds, TaS_2 has a small and size-dependent band gap.[11] We therefore speculate that TaS_2 nanomaterials may possess strong NIR absorption for efficient generation of hyperthermia under laser irradiation. More impressively, bulk TaS_2 is featured by the layered structure and can be exfoliated into single or few-layer sheets by breaking the week Van der Waals force between the adjacent layers.[12] Such a layered sheet structure provides a large surface area for efficient loading of small molecular drugs via multiple intermolecular interactions including **π-π** stacking, Van der Waals force, electrostatic and hydrophobic interactions. Therefore, we expect TaS_2 NSs to be a unique and effective platform for CT imaging-guided combinatorial cancer therapy (Scheme 1).

To this end, we report here, for the first time, a novel Ta-based photothermal agent composed of biocompatible TaS_2 NSs and evaluated their potential as a multifunctional platform for simultaneous NIR hyperthermia, drug delivery, and CT imaging. In this work, we chose doxorubicin (DOX) as a proof of concept test to examine the drug loading capacity and controllable drug release of the TaS_2 NS platform. *In vivo* combinatorial cancer therapy and CT imaging were demonstrated in a mouse xenograft tumor model after systemic delivery. Meanwhile, the *in vivo* toxicity studies of the TaS_2 NS platform were performed to further demonstrate its potential for biomedical applications. We expect this study to lay the foundation for further work to develop safe and efficient Ta-based nanomaterials for theranostic treatment of a wide range of human diseases including cancers.

2. Results and Discussion

2.1. Synthesis and Characterization of PEG-TaS_2 NSs

TaS_2 NSs were first prepared using bulk TaS_2 by combinatorial grinding and sonication processes (Scheme 1A). To improve their physiological stability, 1,2-distearoyl-sn-glycero-3-phosphoethanolamine-N-[methoxy(polyethylene glycol)-3000] (DSPE-PEG) was coated on the surface of TaS_2 NSs, presumably through the hydrophobic interaction and the van der Waals force,[2j,k] to form PEG-TaS_2 NSs. Without DSPE-PEG coating, TaS_2 NSs

rapidly precipitated in water and physiological solutions (Figure 1A). In contrast, PEG-TaS_2 NSs were well-dispersed in water, PBS, and serum without detectable agglomeration. The sheet structure of PEG-TaS_2 was confirmed by TEM (Figure 1B), and the hydrodynamic size of the PEG-TaS_2 NSs was ~110 nm (Figure 1C) as determined by dynamic light scattering (DLS). High-resolution TEM (HRTEM) imaging further revealed lattice fringes with a spacing of ~0.26 nm (Figure 1B), which corresponds to the TaS_2 crystal structure.[13] More impressively, as we hypothesized, these PEG-TaS_2 NSs exhibited broad and dose-dependent absorption ranging from the ultraviolet (UV) to NIR region (Figures 1D and Figure S1).

To evaluate their NIR-induced hyperthermia, PEG-TaS_2 NSs were dispersed in water at different concentrations and exposed to an 808 nm laser at a power density of 2 W/cm^2, and the solution temperature was monitored. Pure water was also used as a reference. Figure 1E shows the temperature increase of pure water and the PEG-TaS_2 NS solutions at different concentrations during laser irradiation. The solution temperature of the PEG-TaS_2 NS solutions increased rapidly and depended on the concentration of PEG-TaS_2 NSs. At a concentration of 0.3 mg/mL, the temperature of the PEG-TaS_2 NS solution was increased by ~35 °C after 10 min irradiation, indicating the high photothermal effect of PEG-TaS_2 NSs. In comparison, the temperature of pure water was increased by < 3 °C, even when the power density was increased to 2.5 W/cm^2 (Figure S2A-C). The photothermal conversion efficiency was determined to be 39% (Figure S2D), which is higher or comparable to many previously reported photothermal nanomaterials (Table S2). We further examined the photostability of PEG-TaS_2 NSs by exposure of PEG-TaS_2 NSs to the NIR laser for three irradiation cycles, and the solution temperature was measured. As can be seen in Figure 1F, no obvious change in the photothermal effects was observed after three cycles of heating and cooling processes at a higher power density of 2.5 W/cm^2, clearly suggesting the high tolerance of PEG-TaS_2 NSs to the laser irradiation.

2.2. Cytotoxicity and Photothermal Cytoxicity

The cytotoxicity of PEG-TaS_2 NSs was examined in HeLa and PC3 cells *in vitro*. The cell viability after treatment of PEG-TaS_2 NSs was first tested using the AlamarBlue assay. Without NIR exposure, treatment of PEG-TaS_2 NSs did not induce significant cytotoxicity in both cell lines at tested concentrations after incubation for 24-48 h (Figures 2A and Figure S3A). The release of lactate dehydrogenase (LDH) in NS-treated cells was similar to the control group (Figure S3B), indicating that the NSs had no influence on the integrality of cell membrane. As introduction of reactive oxygen species (ROS) has been reported to be one key toxicity response of inorganic nanomaterials,[14] we also tested the ROS production in HeLa cells. Figure S3C showed no elevated ROS generation in the NS-treated group vs. control group. All these results indicate the low cytotoxicity of PEG-TaS_2 NSs.

Next, the NIR-triggered cell ablation *in vitro* by PEG-TaS_2 NSs was examined. With Cy5.5-labelled PEG-TaS_2 NSs, we first confirmed that the PEG-TaS_2 NSs were efficiently internalized by cancer cells through caveolae- and clathrin-mediated endocytosis pathways (Figure S4). Then, PEG-TaS_2 NS-treated HeLa or PC3 cells were exposed to NIR irradiation at a power density of 2W/cm^2 for 5 min, and the cell viability was measured after 24 h. A

dose-dependent cell death was noticed, and less than 10% of the NS-treated cells survived upon laser irradiation at a concentration of 0.2 mg/mL or higher (Figure 2B). The live (green) and dead (red) cells in different treatment groups were stained with calcein AM and propidium iodide (PI), respectively, to further confirm the photothermal effect of PEG-TaS_2 NSs triggered by NIR irradiation. Figure 2C showed that the majority of the PEG-TaS_2 NS-treated cells within the laser spot were killed, as indicated by the clear demarcation between the live and dead cells. In contrast, cells treated with laser or PEG-TaS_2 NSs alone showed negligible death (Figure 2C). Moreover, similar results were also observed in HeLa cells (Figure S5), clearly suggesting the great potential of NIR-mediated PTA for safe treatment of different cancers.

2.3. *In Vitro* Drug Delivery

As the large surface-area-to-volume ratio of NSs allows for efficient loading of small molecular drugs via the electrostatic force, **π-π** stacking, or hydrophobic interaction,[2c] DOX was chosen as a proof-of-concept test of the drug loading capacity of PEG-TaS_2 NSs. To do this, PEG-TaS_2 NSs were incubated with increasing concentrations of DOX in PBS buffer (pH 7.4) at room temperature for 24 h, followed by repeated washing. The loading of DOX was monitored based on the absorbance of DOX. The increased absorbance at 480 nm (Figure S6) and the zeta-potential change of PEG-TaS_2 NSs (Table S1) provided solid evidence for DOX loading. The maximum loading efficiency was ~177% by weight (Figure 3A). Notably, for the following experiments unless otherwise specified, we selected the NS formulation with a neutral charge and a favorable drug loading (~112%). Since NSs can release the loaded drugs in response to thermal and acidic stimuli,[15] the release profile of DOX from PEG-TaS_2 NSs was then assessed. As shown in Figure 3B, no obvious DOX release was noticed under physiological pH, vs. ~30% of DOX released at pH 5.0 after 24 h. NIR light also triggered fast release of DOX, as the heat generated by PEG-TaS_2 NSs may reduce their binding with DOX, accelerating the diffusion and dissociation of drug molecules from PEG-TaS_2 NSs. About 50% of DOX was released at pH 7.4 upon laser irradiation, while over 80% release was noticed under pH 5.0 and NIR light during the same period of time of 24 h.

Next, we tested whether the stimuli-responsive PEG-TaS_2 NSs could deliver DOX to tumor cells for combinatorial hyperthermia and chemotherapy. HeLa and PC3 cells were treated with free DOX, PEG-TaS_2, and PEG-TaS_2-DOX at increasing concentrations for cell viability test (Figures 3C and Figure S7). Similar to Figure 2A,B, PEG-TaS_2 treatment alone showed negligible effects on the cell viability, whereas a dose-dependent cell death was observed in the PEG-TaS_2-treated group with laser irradiation. Notably, PEG-TaS_2-DOX NSs were most effective in suppressing cell growth when combined with laser irradiation, resulting in over 90% of cell death at a DOX concentration of 100 μg/mL. As NIR-mediated hyperthermia and chemotherapeutic drugs generally activate the intrinsic/mitochondrial pathway of apoptosis such as p38 MAPK signaling,[16] we also investigated the phosphorylation of p38 protein kinase in cells treated with different groups. As shown in Figure 3D, dramatic activation of apoptotic phospho-p38 (p-p38) was observed in the PEG-TaS_2-DOX-treated group as compared to other groups, which is consistent with the *in vitro* therapeutic results.

2.4. *In Vivo* Pharmacokinetics and Biodistribution

Given these promising *in vitro* results, we proceeded to evaluate whether the heat generated by PEG-TaS_2 NSs under NIR irradiation could improve the systemic delivery of drugs to solid tumors. To do this, we first established the PC3 xenograft tumor model. The pharmacokinetics and biodistribution of the PEG-TaS_2-DOX NSs were then examined to see whether PEG-TaS_2 NSs could deliver DOX to tumors after intravenous injection. Free DOX was also injected into another group of tumor-bearing mice for comparison. As shown in Figure S8A,B, free DOX did not accumulate efficiently in the tumor due to its short blood circulation time. In contrast, PEG-TaS_2-DOX NSs showed significantly prolonged circulation life and higher drug accumulation in the tumor through the EPR effect. More strikingly, the tumor DOX fluorescence intensity in the PEG-TaS_2-DOX-treated group along with laser irradiation was much higher compared to the PEG-TaS_2-DOX-treated group (Figure S8C). It has been suggested that local heating is able to induce several physiological changes within the tumor tissue including increased blood flow, vasodilation, and enhanced vascular permeability, thus leading to improved tumor accumulation of nanomedicines and subsequently yielding more effective delivery of cargos to tumors.[17] It is also worth noting that the heat generated upon NIR irradiation would trigger the release of DOX molecules from the nanomaterial surfaces on which DOX fluorescence is partially quenched. The released DOX could thus also contribute to the bright fluorescence of tumor tissues. Therefore, we speculated that the enhanced fluorescence in tumors from the PEG-TaS_2-DOX+laser group may be ascribed to the increased tumor accumulation of PEG-TaS_2-DOX NSs through heat-dilated tumor vascular permeability and the released DOX from the surface of PEG-TaS_2 NSs, though more experiments will be needed to determine the contribution from each of these two factors.

2.5. *In Vivo* Anti-Tumor Efficacy

Tumor-bearing mice were then divided into six groups. Three groups were intravenously injected with PBS, PEG-TaS_2, and PEG-TaS_2-DOX, respectively, followed by exposure to an 808 nm laser at a power density of 2 W/cm^2 for 5 min. Other control groups included PBS, free DOX and PEG-TaS_2 without NIR exposure. Figure 4A shows that the tumor temperature in the PBS group increased by < 4 °C after NIR irradiation, whereas the tumor temperature in the PEG-TaS_2 or PEG-TaS_2-DOX group was increased by ~24-26 °C to over 60 °C after the same irradiation period. The hyperthermia-induced apoptosis in each group was also examined using terminal deoxynucleotidyl transferase dUTP nick end labeling (TUNEL) assay (Figure 4B). Negligible apoptosis was observed for the PBS, laser, and PEG-TaS_2 groups, and the DOX-treated group showed little apoptosis. In comparison, PEG-TaS_2-treated group with laser irradiation showed obvious apoptosis, and it was even higher for the PEG-TaS_2-DOX-treated group along with laser irradiation. Hematoxylin and eosin staining further confirmed the most obvious tumor necrosis in the PEG-TaS_2-DOX-treated group along with laser irradiation, as compared to other groups (Figure S9).

The tumor size of each group was then measured using a digital caliper every other day for 20 days, and the tumor growth profiles were shown in Figure 4C. The laser- or PEG-TaS_2-treated group showed a similar tumor-growth profile to the PBS group. Free DOX induced a modest inhibition effect on the tumor growth. The tumor growth was remarkably suppressed

in the PEG-TaS_2-treated group with laser irradiation, and more impressively, tumors were completely eliminated in the mice treated with PEG-TaS_2-DOX followed by laser irradiation without causing obvious weight loss (Figures 4C,D and Figure S10). All these results suggest that PEG-TaS_2 NSs may serve as an effective platform for drug delivery and combined cancer hyperthermia and chemotherapy.

2.6. CT Imaging

It has also been increasingly recognized that the EPR effect, the dominant mechanism that mediates the tumor accumulation of nanomaterials, varies among patients and tumor types and even within the same patient/tumor type over time,[18] which highlighted the need to incorporate the imaging function into nanomedicines to identify cancer patients with stronger EPR effects and higher tumor accumulation of nanomedicines for more efficient cancer treatment.[19]

In addition to cancer therapy, PEG-TaS_2 NSs can also be an efficient CT imaging contrast agent, due to the high X-ray attenuation coefficient of Ta.[20] Indeed, the K-edge value of Ta (67 KeV) is located within the highest energy region of the X-ray spectrum (50-70 KeV),[21] thus enabling PEG-TaS_2 NSs to provide high X-ray attenuation. To assess the CT contrast efficiency of PEG-TaS_2 NSs, their X-ray attenuation was first compared to that of iobitridol, a clinically widely used CT contrast agent (Figure 5A,B). Both PEG-TaS_2 NSs and iobitridol exhibited a linear increase in Hounsfield units (HU) value as a function of concentration. The HU values of PEG-TaS_2 NSs were also comparable to those of iobitridol at different operating voltages (100-140 KVp) (Figure S11). To further test the potential for *in vivo* imaging, PC3 tumor-bearing mouse was intravenously injected with PEG-TaS_2 NSs through the tail vein, and time-dependent whole body CT imaging was carried out. Iobitridol is known to be rapidly cleared from the blood within minutes due to its small molecular weight and renal filtration.[21a] In contrast, the CT signal in the heart at 2 h post-injection of PEG-TaS_2 NSs was still much brighter compared to that of pre-injection, indicating their longer circulation life (Figure 5C). Therefore, the NS-based CT imaging can be used for *in vivo* tracking of PEG-TaS_2 NSs as confirmed by the increased HU value of the tumor in Figure 5D, and may potentially be used for imaging-guided drug delivery and the selection of cancer patients with high EPR effect.[5]

2.7. *In Vivo* Toxicity Studies

Finally, the potential *in vivo* toxicity of PEG-TaS_2 NSs was evaluated. Healthy mice were intravenously injected with PBS or PEG-TaS_2 NSs through the tail vein. Serum samples were collected at 24 h post injection for blood and immune analysis. PEG-TaS_2 NS treatment did not alter the serum levels of aspartate aminotransferase (AST), alanine aminotransferase (ALT), albumin, total protein (TP), creatinine, or blood urine nitrogen (BUN) (Figures 6A-F). The levels of IFN-γ, IL-6, and TNF-α were similar to those in the PBS control group (Figure 6G-I), indicating that PEG-TaS_2 NSs did not induce obvious cytokine response. Moreover, no noticeable signal of inflammation or tissue damage was observed in major organs including heart, liver, lung, spleen, and kidney (Figure 6J). Although systematic studies will still be required to understand the long-term toxicity and metabolism

of PEG-TaS_2 NSs, our preliminary toxicity study warrants further exploration of this multifunctional system.

3. Conclusion

In summary, we developed a novel PEG-TaS_2 NS platform for effective and safe cancer therapy. PEG-TaS_2 NSs exhibited strong NIR absorption and efficient generation of hyperthermia upon laser irradiation with a high photothermal conversion efficiency of 39%. Their layered sheet structure also allowed for high loading of small molecular drugs, and the drug release could be triggered by NIR light and acidic pH. The combined hyperthermia and chemotherapy was demonstrated both *in vitro* and *in vivo*, with compelling anti-cancer effect. Our preliminary toxicity studies also suggest that PEG-TaS_2 NSs have nice biocompatibility without inducing immune response and tissue damage. Furthermore, the inherently high X-ray attenuation of Ta makes PEG-TaS_2 NSs attractive as an effective CT imaging contrast agent with prolonged circulation time *in vivo*, indicating their potential use for imaging-guided drug delivery. Despite that our *in vitro* and *in vivo* studies have shown promising anti-cancer and imaging effects, some potential limitations of this PEG-TaS_2 NS platform may be further considered. For instance, the absorption to far-infrared regions may be more beneficial for improving the penetration depth of light and treating the tumors in deeper tissues/organs. In addition, CT imaging alone is suboptimal in tumor definition and lacks functional information, and thus the integration with other imaging modalities may be required to provide more precise imaging guidance in cancer treatment. We expect the PEG-TaS_2 NS platform to pave a new way for developing more effective theranostic nanomedicines to treat a variety of solid tumors.

4. Experimental Section

Materials

Raw TaS_2 materials were purchased from Alfa Aesar. DSPE-PEG (1,2-distearoyl-sn-glycero-3-phosphoethanolamine-N-[methoxy(polyethylene glycol)]) with PEG molecular weight 3000 was obtained from Avanti Polar Lipids. Amine-modified DSPE-PEG (DSPE-PEG-NH_2) with PEG molecular weight 3000 was purchased from Nanocs. N-methyl-2-pyrrolidone (NMP) dimethylformamide (DMF), and chloroform were acquired from Sigma-Aldrich and used directly. Cy5.5 NHS ester was purchased from Lumiprobe. Antibodies used in this work were purchased from Cell Signalling.

Preparation of TaS_2 NSs

The raw TaS_2 materials were dispersed in NMP (2 mL) at a concentration of 50 mg/mL. After grinding for 1 h, the TaS_2 dispersion was diluted with NMP to a total volume of 5 mL and then sonicated for another 1 h in ice-bath at a power of 500 W. Subsequently, the mixture was re-ground for 30 min and then transferred into NMP (10 mL) in a glass vial, followed by sonication for 2 h in ice-bath. The resultant solution was centrifuged at a speed of 3,000 rpm for 5 min to remove the large particles. The suspension was stored at 4 °C for further modification and characterization.

PEG Coating of TaS_2 NSs

For PEG modification, TaS_2 NSs (10 mg) was dispersed in 50 mL of chloroform containing DSPE-PEG (30 mg). After ultra-sonication for 5 min, chloroform was slowly evaporated with a rotary vacuum pump. The as-prepared PEG-TaS_2 NSs were isolated by centrifugation at 14000 rpm, washed with deionized water twice to remove the free DSPE-PEG, and then re-dispersed in PBS for future characterization.

To prepare Cy5.5-labeled PEG-TaS_2 NSs, DSPE-PEG-NH_2 was first conjugated with Cy5.5 NHS ester. Briefly, DSPE-PEG-NH_2 (50 mg) and Cy5.5 NHS ester at a mole ratio of 1:1were dissolved in DMF (10 mL). After reaction at room temperature for 12 h, the mixture was transferred to a dialysis tube and then dialyzed against deionized water for 48 h, followed by freeze-drying under vacuum. The Cy5.5-labed DSPE-PEG and DSPE-PEG (1:4) were then coated on the surface of TaS_2 NSs to generate Cy5.5-labelled PEG-TaS_2 NSs using the aforementioned method.

Drug Loading and Release

For DOX loading, PEG-TaS_2 NSs were dispersed in PBS (0.2 mg/mL) and then mixed with different concentrations of DOX in PBS (0-1 mg/mL). Then, the mixtures were stirred at room temperature for 24 h. Excess DOX was removed by centrifugation and repeated washing with PBS until no color was noticeable in the supernatant. The resulting PEG-TaS_2-DOX NSs were re-dispersed in PBS and the loading efficiency of DOX was determined by the detection of the absorbance at 490 nm.

To investigate drug release kinetics, the solutions of PEG-TaS_2-DOX NSs (2 mg/mL, 3 mL) in PBS buffers with pH 5.4 or pH 7.4 were stirred at 37 °C. At different time intervals, the solutions were treated with vs. without laser irradiation using an 808 nm NIR laser at a power density of 2 W/cm^2 for 5 min. 0.1 mL of NS suspension was taken out at the indicated time interval and centrifuged at 10,000 rpm for 20 min. The released DOX in the supernatant was quantified using UV-vis spectra. The same volume of fresh buffers was then added to the pellet. After sonication, the solution was added back to the residual PEG-TaS_2-DOX NS solutions.

Characterization

The morphology of NSs was characterized using a Tecnai G2 Spirit BioTWIN microscope (FEI Company) operating at 80 kV. The size and surface charge (zeta potential) of PEG-TaS_2 NSs were determined using Dynamic Light Scattering or DLS (15-mW laser, incident beam of 676 nm; Brookhaven Instruments Corporation). UV-vis-NIR absorbance of PEG-TaS_2 NSs was measured using the Synergy HT multi-mode microplate reader (BioTek Instruments Inc.). CT imaging was carried out using a JL U.A NO.2 HOSP Philips iCT 256 slice scanner. The imaging parameters were as follows: thickness, 0.9 mm; pitch, 0.99; 100-140 KVp, 300 mA; field of view, 350 mm; gantry rotation time, 0.5 s; table speed, 158.9 mm/s.

Measurement of Photothermal Performance

To examine the photothermal conversion of PEG-TaS_2 NSs, PEG-TaS_2 dispersion in PBS (2 mL) at different concentrations (0-0.5 mg/mL) were added in quartz vials and respectively irradiated with an 808 nm NIR laser at different power densities (1.5-2.5 W/cm^2) for 10 min. The temperature of the solution was recorded every 10 s using a digital thermometer with a thermocouple probe.

Cell Culture

HeLa and PC3 cells were obtained from ATCC and cultured in RPMI-1640 medium (ATCC) supplemented with 10% (v/v) FBS with high glucose. All cells were maintained at 37 °C in 5% CO_2 and a humidified atmosphere.

In Vitro Toxicity Studies of PEG-TaS_2 NSs

HeLa and PC3 cells were seeded in 96-well plates at a density of 5,000 cells/well. After 24 h incubation, the medium was replaced with fresh medium containing different concentrations of PEG-TaS_2 NSs. After 24 or 48 h incubation, the cell viability was measured using the AlamarBlue assay (Life Technologies) according to the manufacturer's instructions.

HeLa cells were used to investigate the extracellular LDH and the intracellular ROS production. HeLa cells were incubated with different concentrations of PEG-TaS_2 NSs for 24 h. The release of LDH and the ROS production in cells were examined using LDH assay (Life Technologies) and 2,7-dichlorofluorescien diacetate (DCFH-DA) (Life Technologies), respectively, according to the manufacturer's instructions.

In Vitro Photothermal Cytotoxicity

To evaluate the photothermal cytotoxicity of PEG-TaS_2 NSs upon laser irradiation, HeLa and PC3 cells were seeded in 6-well plates and incubated at 37 °C with 5% CO_2 for 24 h. PEG-TaS_2 NSs were then added into the plates with the final concentration of 0.3 mg/mL and incubated for 12 h. Thereafter, the cells were irradiated with an 808 nm laser at a power density of 2 W/cm^2 for 5 min. After incubation at 37 °C for another 3 h, the cells were stained with both calcein AM (calcein acetoxymethyl ester) and PI (propidium iodide) to determine the photothermal cytotoxicity of PEG-TaS_2 NSs by a laser scanning confocal microscope.

To quantify the photothermal cytotoxicity of PEG-TaS_2 NSs under laser irradiation, HeLa and PC3 were plated and incubated in 96-well plates at 37 °C in an atmosphere of 5% CO_2 and 95% air for 24 h. Different concentrations of PEG-TaS_2 NSs were then added (0-0.5 mg/mL), and the cells were incubated for another 12 h. Following irradiation with an 808 nm laser at 2 W/cm^2 for 5 min, the cell viability of HeLa and PC3 cells was determined using the AlamarBlue assay (Life Technologies) according to the manufacture's instruction.

In Vitro Combinatorial Therapy

To test the combined hyperthermia and chemotherapy of PEG-TaS_2-DOX NSs, HeLa and PC3 cells were seeded and incubated in 96-well plates at 37 °C in an atmosphere of 5% CO_2 and 95% air for 24 h. Different concentrations of DOX, PEG-TaS_2, and PEG-TaS_2-DOX

were then added. After 24 h incubation, part of cells treated with PEG-TaS_2 and PEG-TaS_2-DOX were irradiated with an 808 nm laser (2 W/cm^2, 5 min). The cells were then incubated for another 24 h. The cell viability was measured using the AlarmaBlue assay (Life Technologies) according to the manufacture's instructions.

Western Blot Analysis

Proteins were extracted with a modified radioimmunoprecipitation assay lysis buffer (50 mM Tris-HCl pH 7.4, 150 mM NaCl, 1% NP-40 substitute, 0.25% sodium deoxycholate, 1 mM sodium fluoride, 1 mM Na_3VO_4, and 1 mM EDTA), which is supplemented with protease inhibitor cocktail (Cell Signaling) and phenylmethanesulfonyl fluoride (1mM). The protein concentrations were quantified using a bicinchoninic acid protein assay kit (Pierce/Thermo Scientific) according to the manufacturer's instructions. Equal amounts of protein were loaded in SDS-PAGE gels and then transferred to the polyvinylidenedifluoride membrane. After blocking with BSA (3%) in TBST (50 mM Tris-HCl, pH 7.4 and 150 mM NaCl, and 0.1% Tween 20) for 1 h, the blots were incubated with primary antibodies overnight at 4 °C under moderate shaking. Signals were detected using horseradish peroxidase-conjugated secondary antibodies and an enhanced chemiluminescence (ECL) detection system (Pierce).

Animals

Animals were provided by the Charles River Laboratories. All animal experiments and procedures were performed in accordance with National Institutes of Health animal care guidelines. Animal protocols were approved by the Institutional Animal Care and Use Committees on Animal Care (Harvard Medical School).

Pharmacokinetic Study

For the *in vivo* pharmacokinetic study, healthy C57BL/6 mice were intravenously injected with free DOX or PEG-TaS_2-DOX (4.5 mg/kg PEG-TaS_2 and 5 mg/kg DOX) through the tail vein. At different time intervals, blood (20 μL) was collected by a retro-orbital puncture. The fluorescence of DOX in the blood was measured using the BioTekmicroplate reader.

Xenograft Tumor Model

5×10^6 PC3 cells were suspended in FBS-free RPMI-1640 medium (200 μL) and then subcutaneously implanted on the bilateral flanks of 4-week-old male athymic nude mice. Mice were used for the following *in vivo* experiments when the tumor volume reached 50-100 mm^3.

Biodistribution Study

For the *in vivo* biodistribution study, the PC3 tumor-bearing mice were intravenously injected with free DOX or PEG-TaS_2-DOX NSs at a DOX concentration of 5mg/kg through the tail vein. At 30 min after injection, the tumors in PEG-TaS_2-DOX-treated mice were then irradiated with an 808 nm laser for 5 min. For comparison, another group of PC3 tumor-bearing mice was intravenously injected with PEG-TaS_2-DOX NSs at the same DOX

concentration of 5mg/kg without laser irradiation. After 24 h, the mice were sacrificed and the tumors were collected for imaging.

In Vivo Monitoring Tumor Temperature

Twenty-four hours after intravenous injection of PBS, PEG-TaS_2 (4.5 mg/kg), or PEG-TaS_2-DOX (4.5 mg/kg PEG-TaS_2 and 5 mg/kg DOX), tumor-bearing mice were exposed to an 808 nm laser at a power density of 2 W/cm^2 for 5 min. The temperature of the tumor was monitored every minute using an NIR thermal camera (Fluke).

In Vivo Therapeutic Efficacy

When the tumor size reached 50-100 mm^3, mice were randomly divided into six treatment groups (5 mice for each group) including (i) PBS, (ii) laser, (iii) PEG-TaS_2 (4.5 mg/kg), (iv) free DOX (5 mg/kg), (v) PEG-TaS_2 (4.5mg/kg)+laser, and (vi) PEG-TaS_2-DOX (4.5 mg/kg PEG-TaS_2 and 5 mg/kg DOX)+laser. After treatment, the tumor size of each group was measured with a caliper every other day. The tumor volume was calculated as: volume = tumor length×(tumor width)^2/2. Relative tumor volumes were used as V/V_0 (V_0 was the tumor volume when the treatment was initiated).

Hematologic Examination and Immune Response

For the *in vivo* toxicity study, healthy C57BL/6 mice were intravenously administered with 200 μL of PBS or PEG-TaS_2 NSs dispersed in PBS (10 mg/mL) through the tail vein. One month after injection, the organs were harvested, fixed in a 10% formalin solution, and embedded in paraffin for hematoxylin and eosin (H&E) staining.

For immune analysis, immunocompetent C57BL/6 mice were intravenously administered 200 μL of PBS or PEG-TaS_2 NSs dispersed in PBS (10 mg/mL) through the tail vein. At 24 h post-injection, representative cytokines including TNF-α, IL-6, and IFN-γ in the serum were determined by enzyme-linked immunosorbent assay or ELISA (PBL Biomedical Laboratories and BD Biosciences) according to the manufacturer's instructions. Serum levels of aspartate aminotransferase (AST), alanine ami-notransferase (ALT), albumin, total protein (TP), creatinine, and blood urine nitrogen (BUN) were also measured.

Supplementary Material

Refer to Web version on PubMed Central for supplementary material.

Acknowledgments

This work was supported by NIH CA200900 and CA160350, and PCF Young Investigator Award. Y. Liu and X. Ji contributed equally to this work.

References

1. a) Zou L, Wang H, He B, Zeng L, Tan T, Cao H, He X, Zhang Z, Guo S, Li Y. Theranostics. 2016; 6:762–772. [PubMed: 27162548] b) Li C. Nat Mater. 2014; 13:110–115. [PubMed: 24452345]
2. a) Shanmugam V, Selvakumar S, Yeh CS. Chem Soc Rev. 2014; 43:6254–6287. [PubMed: 24811160] b) Chimene D, Alge DL, Gaharwar AK. Adv Mater. 2015; 27:7261–7284. [PubMed:

26459239] c) Yang K, Feng L, Shi X, Liu Z. Chem Soc Rev. 2013; 42:530–547. [PubMed: 23059655] d) Qin Z, Bischof JC. Chem Soc Rev. 2012; 41:1191–1217. [PubMed: 21947414] e) Huang X, El-Sayed IH, Qian W, El-Sayed MA. J Am Chem Soc. 2006; 128:2115–2120. [PubMed: 16464114] f) Liu Y, Ai K, Liu J, Deng M, He Y, Lu L. Adv Mater. 2013; 25:1353–1359. [PubMed: 23280690] g) Kam NW, O'Connell M, Wisdom JA, Dai H. Proc Natl Acad Sci U S A. 2005; 102:11600–11605. [PubMed: 16087878] h) Wang J, Zhu G, You M, Song E, Shukoor MI, Zhang K, Altman MB, Chen Y, Zhu Z, Huang CZ, Tan W. ACS nano. 2012; 6:5070–5077. [PubMed: 22631052] i) Miao W, Kim H, Gujrati V, Kim JY, Jon H, Lee Y, Choi M, Kim J, Lee S, Lee DY, Kang S, Jon S. Theranostics. 2016; 6:2367–2379. [PubMed: 27877241] j) Tao W, Ji X, Xu X, Islam M, Li Z, Chen S, Saw PE, Zhang H, Bharwani Z, Guo Z, Shi J, Farokhzad OC. Angew Chem Int Ed. k) Robinson JT, Tabakman SM, Liang Y, Wang H, Casalongue HS, Vinh D, Dai H. J Am Chem Soc. 2011; 133:6825–6831. [PubMed: 21476500]

3. a) Maeda H, Nakamura H, Fang J. Adv Drug Deliv Rev. 2013; 65:71–79. [PubMed: 23088862] b) Farokhzad OC, Langer R. ACS nano. 2009; 3:16–20. [PubMed: 19206243]
4. a) Huang X, Tang S, Mu X, Dai Y, Chen G, Zhou Z, Ruan F, Yang Z, Zheng N. Nat Nanotechnol. 2011; 6:28–32. [PubMed: 21131956] b) Zhou W, Gao X, Liu D, Chen X. Chem Rev. 2015; 115:10575–10636. [PubMed: 26114396] c) Yang W, Guo W, Le W, Lv G, Zhang F, Shi L, Wang X, Wang J, Wang S, Chang J, Zhang B. ACS nano. 2016; 10:10245–10257. [PubMed: 27791364] d) Chen C, Wang S, Li L, Wang P, Chen C, Sun Z, Song T. Biomaterials. 2016; 104:352–360. [PubMed: 27487574] e) Boisselier E, Astruc D. Chem Soc Rev. 2009; 38:1759–1782. [PubMed: 19587967] f) Wang S, Li X, Chen Y, Cai X, Yao H, Gao W, Zheng Y, An X, Shi J, Chen H. Adv Mater. 2015; 27:2775–2782. [PubMed: 25821185]
5. a) Shi J, Kantoff PW, Wooster R, Farokhzad OC. Nat Rev Cancer. 2017; 17:20–37. [PubMed: 27834398] b) Chen H, Zhang W, Zhu G, Chen X, Xie J. Rethinking Cancer Nanotheranostics. Nat Rev Materials. 2017; 2:1–18.
6. Chen X, Gambhir SS, Cheon J. Acc Chem Res. 2011; 44:841. [PubMed: 22004477]
7. Ng KK, Weersink RA, Lim L, Wilson BC, Zheng G. Angew Chem Int Ed. 2016; 55:10003–10007.
8. a) Zheng T, Li GG, Zhou F, Wu R, Zhu JJ, Wang H. Adv Mater. 2016; 28:8218–8226. [PubMed: 27459898] b) Chen W, Ouyang J, Liu H, Chen M, Zeng K, Sheng J, Liu Z, Han Y, Wang L, Li J, Deng L, Liu YN, Guo S. Adv Mater. 2017; 29:1603864.c) Park H, Yang J, Lee J, Haam S, Choi IH, Yoo KH. ACS Nano. 2009; 3:2919–2926. [PubMed: 19772302] d) Zhou Z, Hu K, Ma R, Yan Y, Ni B, Zhang Y, Wen L, Zhang Q, Cheng Y. Adv Funct Mater. 2016; 26:5971–5978.e) Qiu L, Chen T, Öçsoy I, Yasun E, Wu C, Zhu G, You M, Han D, Jiang J, Yu R, Tan W. Nano Lett. 2015; 15:457–463. [PubMed: 25479133]
9. a) Yin W, Yan L, Yu J, Tian G, Zhou L, Zheng X, Zhang X, Yong Y, Li J, Gu Z, Zhao Y. ACS nano. 2014; 8:6922–6933. [PubMed: 24905027] b) Cheng L, Liu J, Gu X, Gong H, Shi X, Liu T, Wang C, Wang X, Liu G, Xing H, Bu W, Sun B, Liu Z. Adv Mater. 2014; 26:1886–1893. [PubMed: 24375758] c) Wang S, Chen Y, Li X, Gao W, Zhang L, Liu J, Zheng Y, Chen H, Shi J. Adv Mater. 2015; 27:7117–7122. [PubMed: 26447460] d) Shen S, Chao Y, Dong Z, Wang G, Yi X, Song G, Yang K, Liu Z, Cheng L. Adv Funct Mater. 2017:1700250.e) Kalantar-zadeh K, Ou JZ, Daeneke T, Strano MS, Pumera M, Gras SL. Adv Funct Mater. 2015; 25:5086–5099.f) Gong L, Yan L, Zhou R, Xie J, Wu W, Gu Z. J Mater Chem B. 2017; 5:1873–1895.
10. a) Black J. Clin Mater. 1994; 16:167–173. [PubMed: 10172264] b) Song G, Chen Y, Liang C, Yi X, Liu J, Sun X, Shen S, Yang K, Liu Z. Adv Mater. 2016; 28:7143–7148. [PubMed: 27275921]
11. Nguyen TP, Choi S, Jeon JM, Kwon KC, Jang HW, Kim SY. J Phys Chem C. 2016; 120:3929–3935.
12. Tan C, Zhang H. Chem Soc Rev. 2015; 44:2713–2731. [PubMed: 25292209]
13. Zhang X, Lai Z, Liu Z, Tan C, Huang Y, Li B, Zhao M, Xie L, Huang W, Zhang H. Angew Chem Inter Ed. 2015; 54:5425–5428.
14. Auffan M, Rose J, Bottero JY, Lowry GV, Jolivet JP, Wiesner MR. Nat Nanotechnol. 2009; 4:634–641. [PubMed: 19809453]
15. Liu T, Wang C, Gu X, Gong H, Cheng L, Shi X, Feng L, Sun B, Liu Z. Adv Mater. 2014; 26:3433–3440. [PubMed: 24677423]
16. a) Hernandez Losa J, Parada Cobo C, Guinea Viniegra J, Sanchez-Arevalo Lobo VJ, Ramon y Cajal S, Sanchez-Prieto R. Oncogene. 2003:22, 3998–4006.b) Ali MR, Rahman MA, Wu Y, Han

T, Peng X, Mackey MA, Wang D, Shin HJ, Chen ZG, Xiao H, Wu R, Tang Y, Shin DM, El-Sayed MA. Proc Natl Acad Sci USA. 2017; 114:E3110–E3118. [PubMed: 28356516]

17. a) Frazier N, Ghandehari H. Biotechnol Bioeng. 2015; 112:1967–1983. [PubMed: 25995079] b) Durymanov MO, Rosenkranz AA, Sobolev AS. Theranostics. 2015; 5:1007–1020. [PubMed: 26155316] c) Gao H, Bi Y, Chen J, Peng L, Wen K, Ji P, Ren W, Li X, Zhang N, Gao J, Chai Z, Hu Y. ACS Appl Mater Interfaces. 2016; 8:15103–15112. [PubMed: 27227416] d) Park JH, von Maltzahn G, Ong LL, Centrone A, Hatton TA, Ruoslahti E, Bhatia SN, Sailor MJ. Adv Mater. 2010; 22:880–885. [PubMed: 20217810]
18. a) Prabhakar U, Maeda H, Jain RK, Sevick-Muraca EM, Zamboni W, Farokhzad OC, Barry ST, Gabizon A, Grodzinski P, Blakey DC. Cancer Res. 2013; 73:2412–2417. [PubMed: 23423979] b) Liu Y, Gunda V, Zhu X, Xu X, Wu J, Askhatova D, Farokhzad OC, Parangi S, Shi J. Proc Natl Acad Sci U S A. 2016; 113:7750–7755. [PubMed: 27342857]
19. a) Miller MA, Gadde S, Pfirschke C, Engblom C, Sprachman MM, Kohler RH, Yang KS, Laughney AM, Wojtkiewicz G, Kamaly N, Bhonagiri S, Pittet MJ, Farokhzad OC, Weissleder R. Sci Transl Med. 2015; 7:314ra183.b) Arrieta O, Medina LA, Estrada-Lobato E, Ramirez-Tirado LA, Mendoza-Garcia VO, de la Garza-Salazar J. Cancer Chemoth Pharm. 2014; 74:211–215.
20. Oh MH, Lee N, Kim H, Park SP, Piao Y, Lee J, Jun SW, Moon WK, Choi SH, Hyeon T. J Am Chem Soc. 2011; 133:5508–5515. [PubMed: 21428437]
21. a) Liu Y, Ai K, Liu J, Yuan Q, He Y, Lu L. Angew Chem Int Ed. 2012; 51:1437–1442.b) Liu Y, Ai K, Lu L. Acc Chem Res. 2012; 45:1817–1827. [PubMed: 22950890]

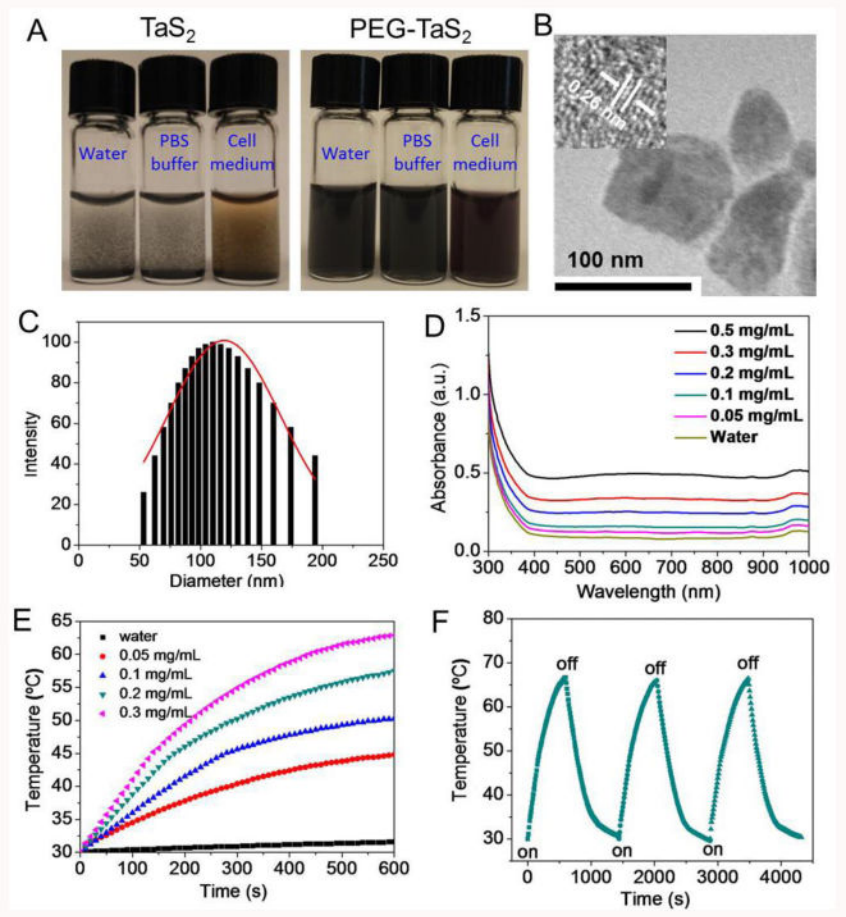

Figure 1.

(A) Digital photos of the TaS_2 NS dispersion in different solutions before vs. after PEG coating. (B) TEM image of PEG-TaS_2 NSs. The insert shows the corresponding HRTEM image. (C) DLS analysis of PEG-TaS_2 NSs. (D) UV-vis-NIR absorption spectra of water and aqueous dispersions of PEG-TaS_2 NSs, and (E) their photothermal heating curves under irradiation by an 808 nm laser (2 W/cm^2, 10 min). (F) Photothermal conversion stability of PEG-TaS_2 NSs. The laser was turned on for 500 s and then turned off for each cycle. The concentration of PEG-TaS_2 NSs is 0.2 mg/mL and the laser power density is 2.5 W/cm^2.

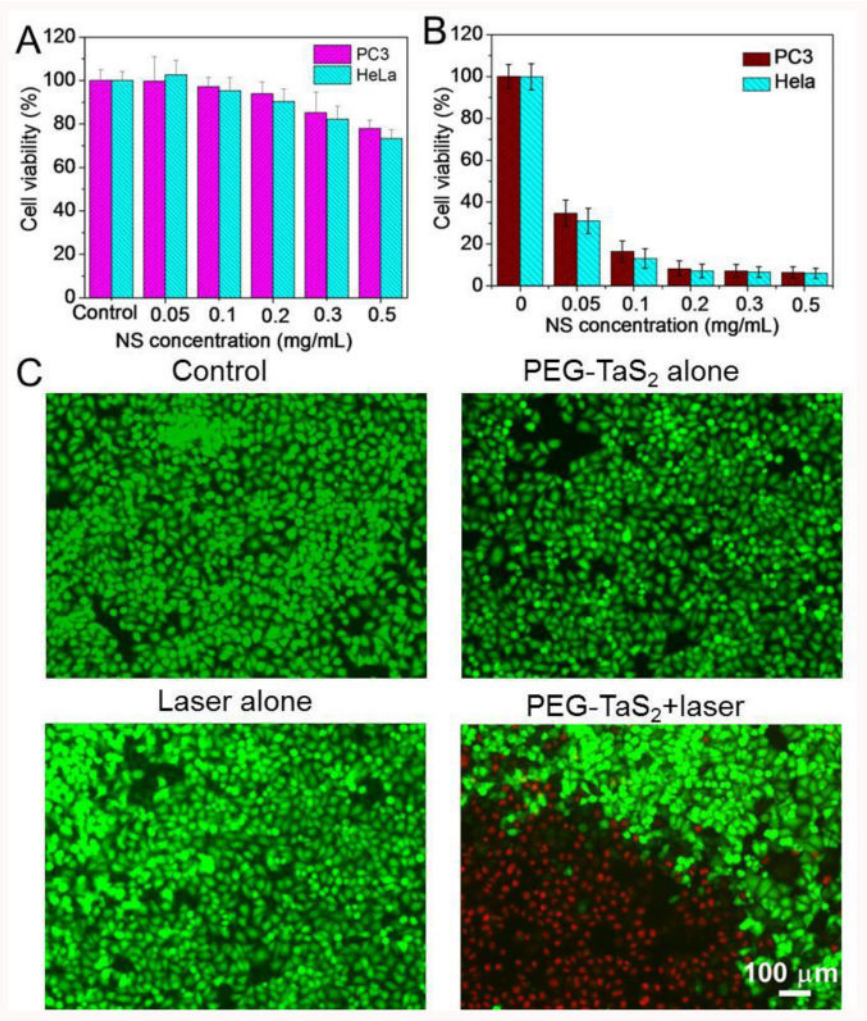

Figure 2.

(A) Cell viability of HeLa and PC3 cells after incubation with different concentrations of PEG-TaS_2 NSs for 24 h. (B) Cell viability of HeLa and PC3 cells treated with different concentrations of PEG-TaS_2 NSs and laser irradiation (808 nm, 2 W/cm^2, 5 min). (C) Confocal image of calcein AM (green) and PI (red) co-stained PC3 cells after treatment with various groups.

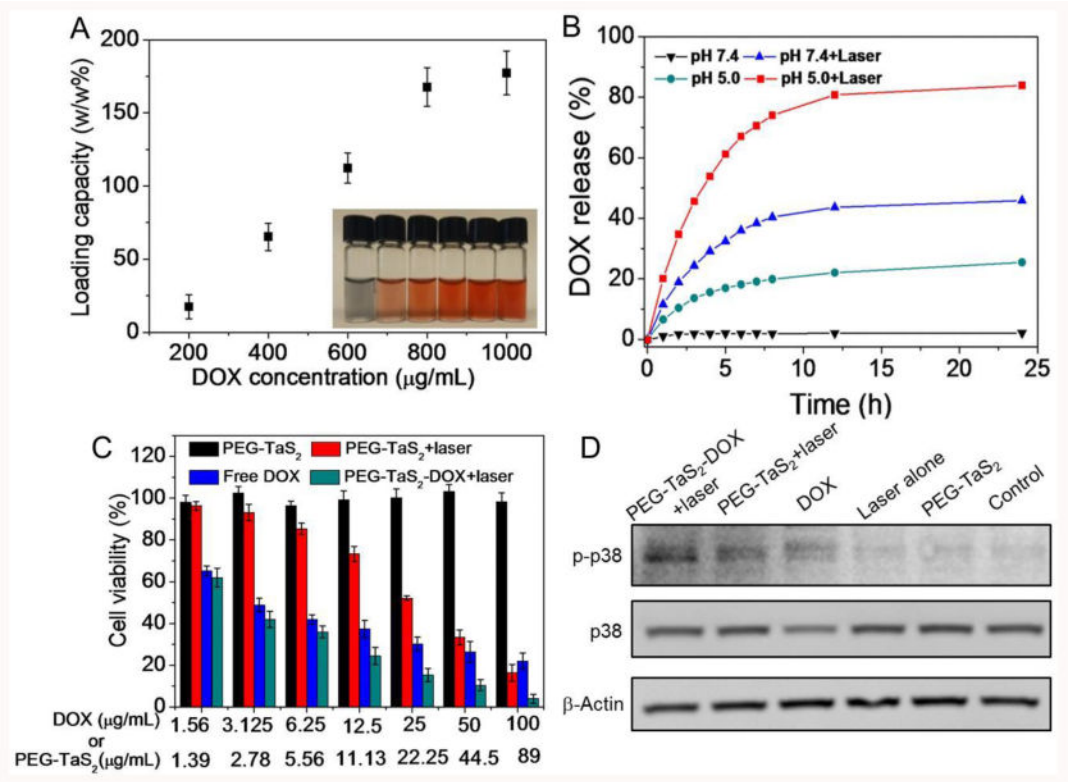

Figure 3.

(A) DOX loading efficiency of PEG-TaS_2 NSs. The insert shows the picture of aqueous dispersions of PEG-TaS_2 NSs with increased DOX loading efficiency. (B) DOX release from PEG-TaS_2 NSs under different conditions. (C) Cell viability of PC3 cells after treatment with various groups. (D) Western blot analysis of phospho-p38 (p-p38) and p38 expression in PC3 cells after treatments with various groups.

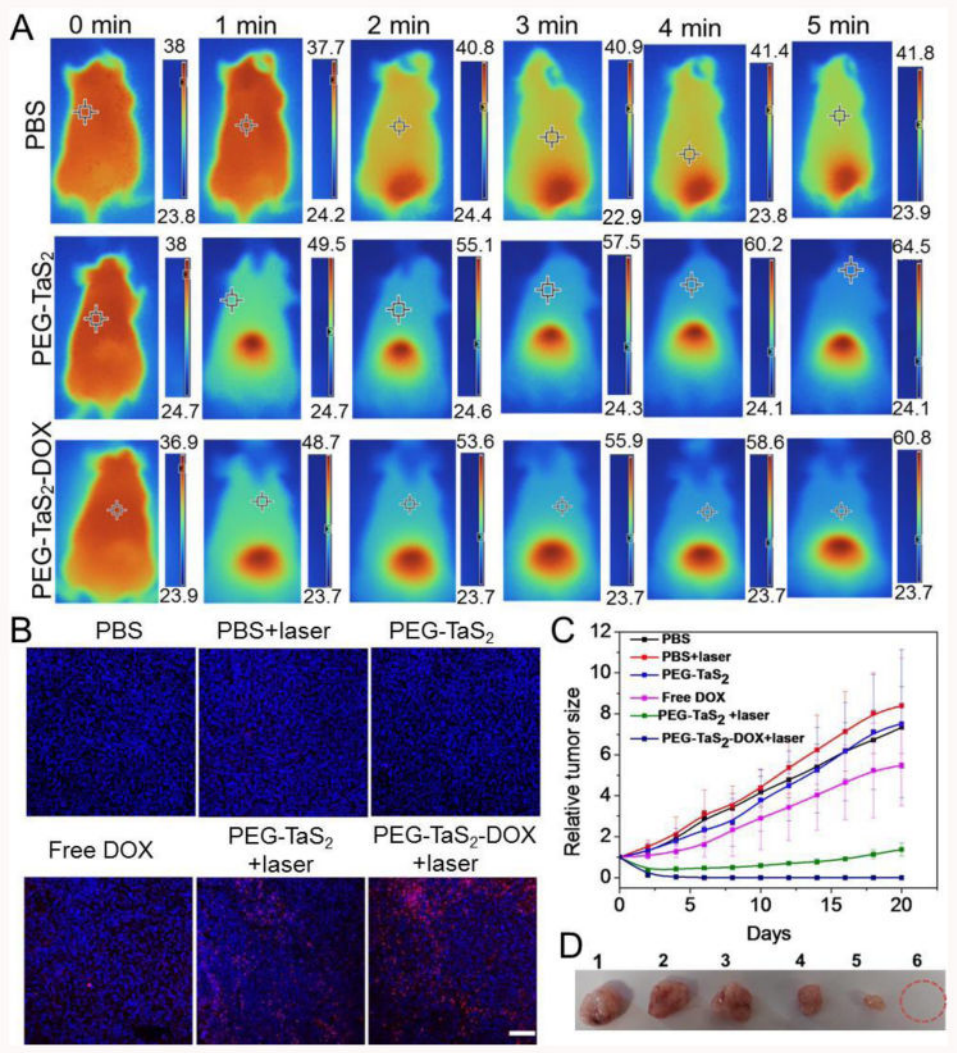

Figure 4.

(A) Thermal images of tumor-bearing mice after treatment with PBS, PEG-TaS_2 NSs, and PEG-TaS_2-DOX NSs followed by laser irradiation. Please note that the scale bar is different for each image. (B) TUNEL staining of tumor tissues (the scale bar is 100 μm) and (C) tumor growth curves of mice from different treatment groups. (D) Photograph of representative tumors from C. Form 1 to 6: PBS group, PBS+laser group, PEG-TaS_2 group, free DOX group, PEG-TaS_2+laser group, and PEG-TaS_2-DOX+laser group.

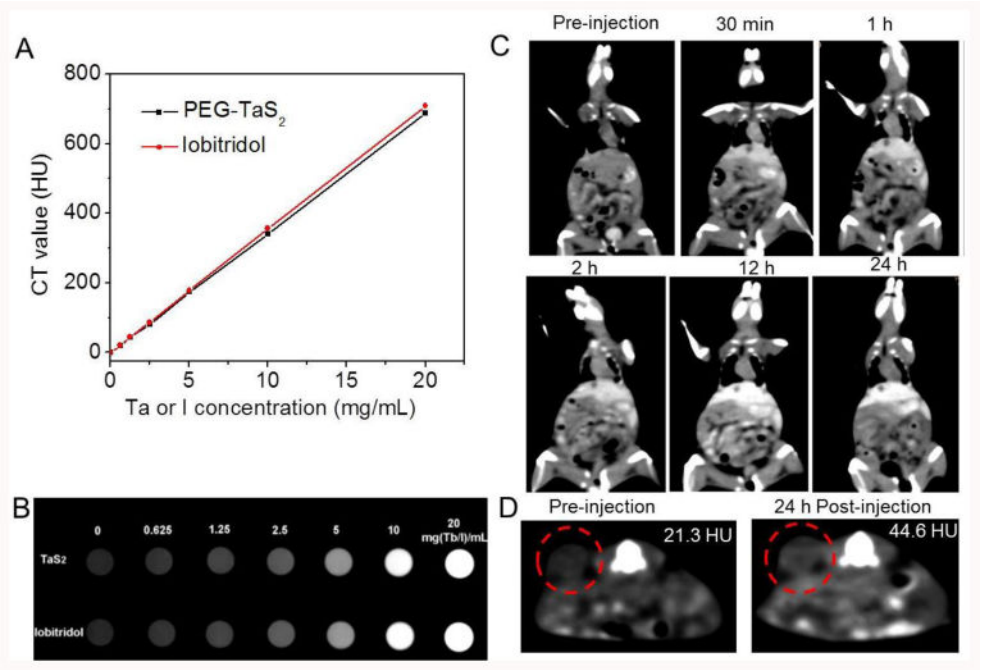

Figure 5.

(A) CT values (HU) of PEG-TaS_2 NSs (black) and iobitridol (red) as a function of the Ta or I concentration at 120 KVp. (B) The corresponding CT image of samples from A. (C) Time-dependent whole body CT imaging of the tumor-bearing mouse after i.v. injection of PEG-TaS_2 NSs. (D) CT imaging and HU value of the tumor before vs. 24 h post injection of PEG-TaS_2 NSs. The red circle indicates the tumor.

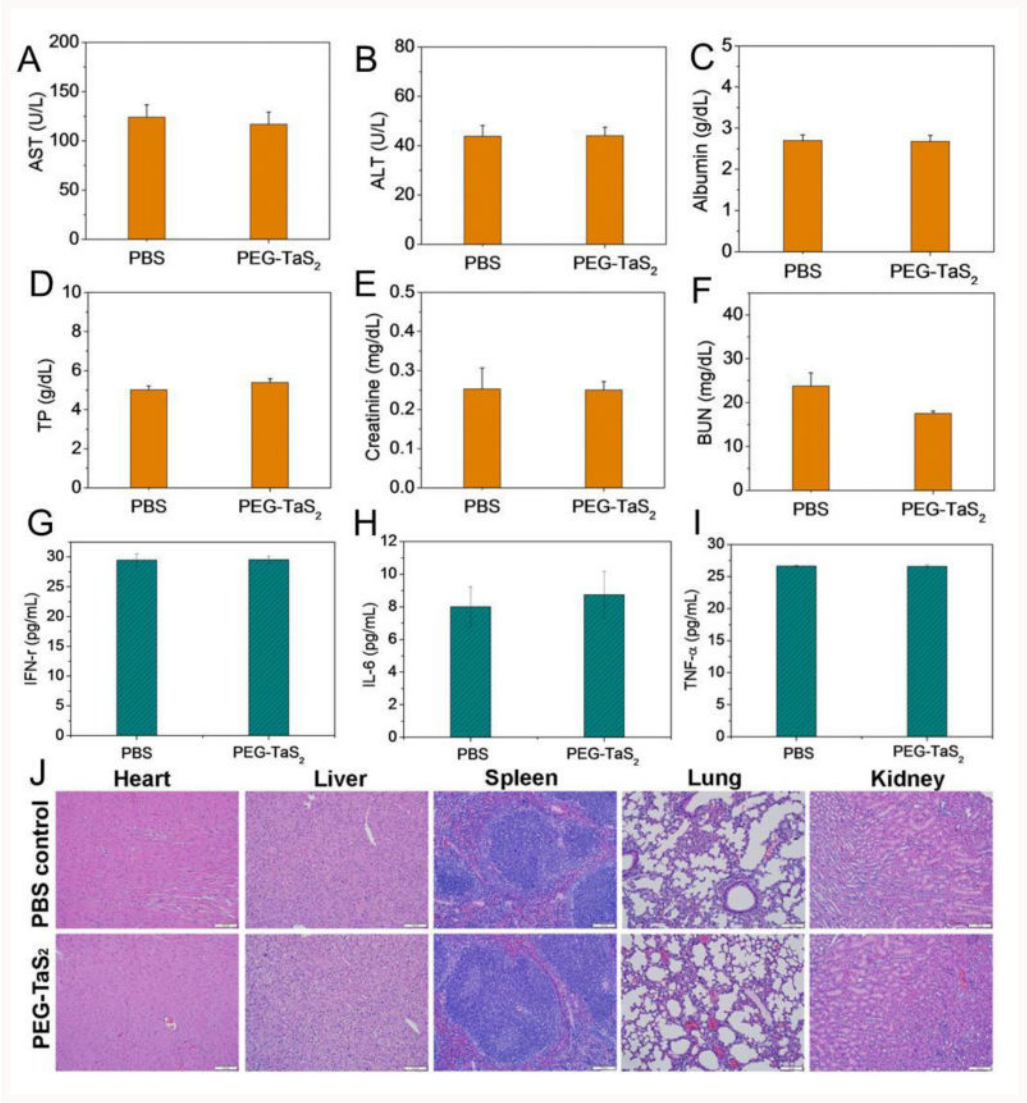

Figure 6.

Serum levels of (A) aspartate aminotransferase (AST), (B) alanine aminotransferase (ALT), (C) albumin, (D) total protein (TP), (E) creatinine, (F) blood urine nitrogen (BUN), (G) IFN-γ, (H) IL-6, and (I) TNF-α in the healthy mice at 24 h after i.v. injection of PBS vs. PEG-TaS_2 NSs. (J) H&E-stained tissue sections of major organs from mice treated with saline vs. PEG-TaS_2 NSs. Images were taken under 20× objective.

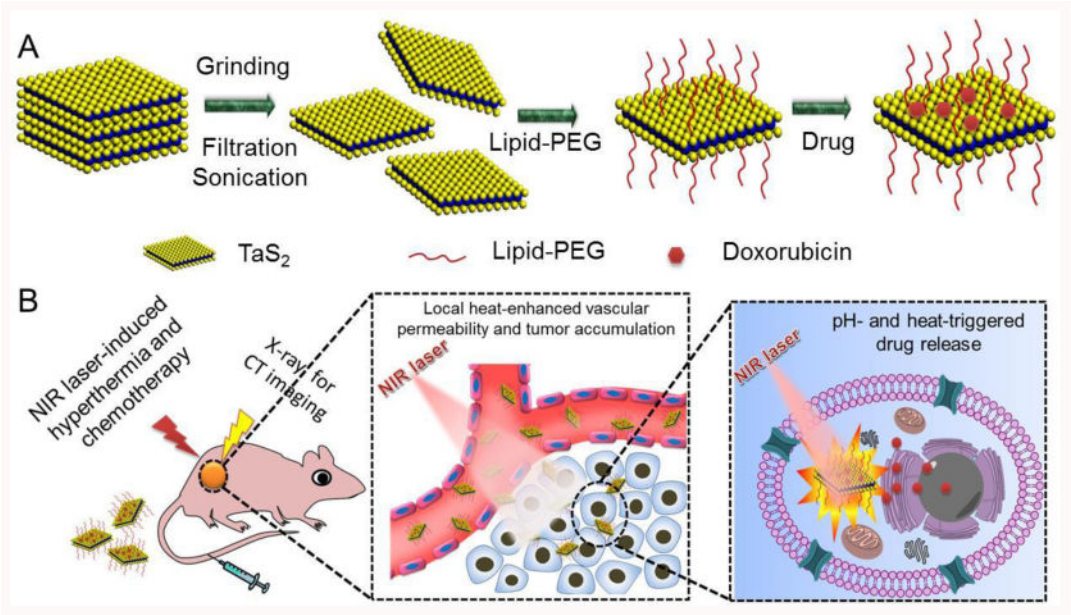

Scheme 1.

Schematic illustration of (A) the synthesis and (B) the multifunctions of PEG-TaS_2 NSs.